Application of poled electro-optic polymer films in a gap-free broadband terahertz system

Zheng, Xuemei, Sinyukov, Alexander, Leahy-Hoppa, Megan, Hayden, L. Michael

Xuemei Zheng, Alexander M. Sinyukov, Megan R. Leahy-Hoppa, L. Michael Hayden, "Application of poled electro-optic polymer films in a gap-free broadband terahertz system," Proc. SPIE 5935, Linear and Nonlinear Optics of Organic Materials V, 59350N (18 August 2005); doi: 10.1117/12.613927

SPIE.

Event: Optics and Photonics 2005, 2005, San Diego, California, United States

Application of poled electro-optic polymer films in a gap-free, broadband terahertz system

Xuemei Zheng, Alexander M. Sinyukov, Megan R. Leahy-Hoppa, and L. Michael Hayden
Department of Physics, University of Maryland, Baltimore County, MD USA 21250

ABSTRACT

We report on the application of poled electro-optic (EO) polymer films in a gap-free, broadband terahertz (THz) system. Using polymer films consisting of 40% Lemke/60% APC (LAPC) as an emitter-sensor pair and a Ti:sapphire regenerative laser pulse amplifier operated at 800-nm-wavelength, we generated and detected transient THz waves, via the optical rectification and EO effect, respectively. We obtained ~12-THz bandwidth from this system with no absorption gaps. The absence of resonant absorption gaps normally seen in THz systems based on crystalline EO materials is attributed to the amorphous form of the polymer films, making our EO polymer emitter-sensor pair advantageous over EO crystals in a gap-free, broadband THz time-domain-spectroscopy (THz-TDS) system. A model has been developed to simulate the spectrum from THz systems and the simulation results were compared with the experimental results. We also report our experiments and simulations for the pulsed THz waves generated by a EO polymer film consisting of 40% DCDHF-6-V/60% APC (DAPC) and detected either by an 80-μm ZnCdTe or a 2-mm ZnTe sensor, with 1300-nm-wavelength pulses from an optical parametric amplifier (OPA). In addition, with the help of our model, we propose employing a wavelength tuning technique to achieve good phase-matching for polymer emitter/sensor pairs, which should lead to very broad bandwidth.

Keywords: electro-optic polymer, THz generation, THz detection, optical rectification, electro-optic sampling, phase-match.

1. INTRODUCTION

The terahertz (THz) frequency region fills the spectral gap between far infrared light and microwave radiation. It has always been recognized that THz spectroscopy is critical to the characterization of far infrared properties of materials. Lattice resonance in dielectric crystals, rotational and vibrational resonances and thermal-emission lines of molecules all occur in the THz region. However, THz spectroscopy was hindered by the low brightness of incoherent far-infrared sources and poor sensitivity of bolometric detectors for quite a long time. Since the 1980s, with the advent of commercially available subpicosecond lasers, using ultrashort laser pulses to generate and detect pulsed THz radiation in a coherent manner has attracted a lot of attention. A lot of work has been done to seek efficient THz emitters and sensitive THz sensors. In general, either radiating photoconductive dipole antennae (PDA)[1,2] or nonlinear electro-optic (EO) materials[3] are employed for THz emitters. As for the THz sensors, PDAs are used in the scheme of photoconductive sampling[1,2] and EO materials are used in the scheme of free-space EO sampling.[4] An optoelectronic THz system with a PDA emitter-sensor pair is generally considered to be more efficient and sensitive than an all-optical THz system with an EO emitter-sensor pair. However, with the development of THz techniques such as THz time-domain spectroscopy (THz-TDS), optical-pump/THz-probe, and THz imaging and tomography, and their applications in fundamental materials studies, biological science, as well as medical diagnosis, the bandwidth of THz systems becomes an important issue, since richer and more complete information can be extracted from a broader bandwidth. All-optical THz systems outperform optoelectronic ones on bandwidth.[5,6,7] For the former, use of an extremely thin EO material has produced >100 THz observable bandwidth, by Kubler *et al*.,[7] while for the latter, bandwidth of ~ 15 THz was report by Shen *et al*. using a pair of low-temperature-grown-GaAs PDAs and a 15-fs laser.[8]

However, lattice resonance existing in both photoconductors and crystalline EO materials results in strong dispersion and absorption gaps in all the reported >10-THz-bandwidth THz systems. When such systems are used for material characterization or for identification of spectral fingerprints of samples under study, information in these gaps cannot be extracted. On the other hand, EO polymers have been under intensive study since the late 1980s, driven by the telecommunication industry crying for cheap EO devices and easy integration. EO polymers with both high EO

Linear and Nonlinear Optics of Organic Materials V, edited by Manfred Eich,
Proceedings of SPIE Vol. 5935 (SPIE, Bellingham, WA, 2005) · 0277-786X/05/$15 · doi: 10.1117/12.613927

coefficients and high glass transition temperature (good thermal stability) are available now.[9] THz technology also benefits from this advancement. EO polymers have been used as THz emitters and THz sensors. Very efficient THz emitters based on different EO polymers have been reported,[10,11] with the high efficiency attributed to the large molecular polarizabilities of the EO polymers. As for THz sensors, the feature of their broadband response has been especially stressed.[12] Because of the lack of a lattice structure, the phonon effect does not exist for EO polymers. This property, together with the low material dispersion in EO polymers, makes it possible to obtain broadband THz radiation free of spectral gaps from a polymer THz emitter-sensor pair. Recently, using such a polymer emitter-sensor pair, we successfully achieved a gap-free THz spectrum with frequency components up to ~12 THz.

At this point, it is crucial to develop a model to guide our selection/synthesis of EO polymers for THz emitters and sensors, with an eye on balancing brightness and broad bandwidth. Thus, we present a model based on optical rectification (OR) and the EO effect to predict the performance of a THz system with a polymer emitter-sensor pair. We then compare the modeling results with our experimental results.

Ultrashort fiber lasers operating at telecommunication wavelengths have been under extensive development for the past decade. They are getting cheaper and smaller every day. As mentioned above, various EO polymers were originally synthesized for telecommunication applications. It will be very interesting to investigate the possibility of employing polymer films in a THz system with a telecommunication-wavelength light source. Success will lead to polymer waveguiding emitters, and probably, all-integrated THz systems in future. In this work, we operated an optical parametric amplifier (OPA) at a wavelength of 1300 nm and used it to pump an EO polymer to generate THz radiation. Further more, based on our modeling work, we propose tuning the output wavelength of the OPA to achieve good phase-matching in a polymer emitter-sensor pair of a THz system.

The structure of this paper is as follows: the preparation of EO polymer films and the characterization of their optical properties are described in Sec. 2; all the experiments with our THz system based on EO polymer films are presented in Sec. 3; the modeling work and the comparison with the experiments are presented in Sec. 4; and Sec. 5 is devoted to a discussion where we propose the future work.

2. MATERIAL FABRICATION AND CHARACTERIZATION

We worked with two EO polymers. The first one is a guest-host mixture of 40% (3-(2-(4-(N,N-diethylamino)-phenyl)ethenyl)-5,5-dimethyl-1,2-cyclohexenylidene)-propanedinitrile (Lemke), with the chemical structure shown in Fig. 1(a), and 60% amorphous polycarbonate (APC). We refer to this material as LAPC. The other one is a guest-host mixture of 40% DCDHF-6-V, with the chemical structure shown in Fig. 1(b), and 60% APC. We refer to this material as DAPC. The preparation of our materials has been described elsewhere.[10,11] Briefly, films were cast from solution onto indium tin oxide coated glass substrates. After solvent evaporation, two solid polymer films were pressed in vacuum 70 ^{o}C above its glass transition temperature T_g for 10 ~ 15 minutes. The thickness of the resulting film was controlled by appropriate polyimide spacers. Films with thickness in the range of 50-350 μm can be obtained with this method. In this work, all the polymer films used were 70 μm thick. All the polymer films were poled normal to the film surface with high electric field (~ 90 V/μm) while being heated up to T_g to achieve the polar order, essential for creating the high 2nd-order nonlinear optical susceptibility. The films were then cooled down to the room temperature, with the external poling voltage still applied, to freeze in the orientation of the chromophores. After fabricating the film sandwiches, we used an ellipsometric technique to measure the EO coefficients of the films. EO coefficients between 25 and 40 pm/V were routinely achieved for LAPC films, and EO coefficients between 40 and 50 pm/V were routinely achieved for DAPC, at wavelength of 800 nm. LAPC and DAPC exhibit peak absorption around 512 nm and 610 nm, respectively. We did not observe significant degradation of the THz performance of the EO polymer films over a few weeks.

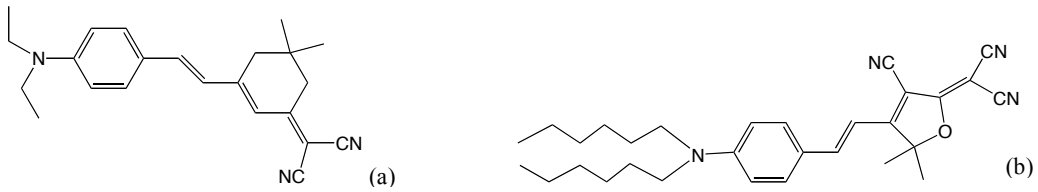

Figure 1: Chemical structure of the dye molecules, (a) LAPC and (b) DAPC.

We measured the refractive indices of LAPC (open circles of Fig. 2) and DAPC (closed circles of Fig. 2) at 785 nm, 1064 nm, 1319 nm, and 1550 nm, respectively. By fitting our experimental data to a Sellmeier dispersion formula, the dispersion of LAPC can be expressed as:

$$n_{opt}{}^2 = 2.3045 + \frac{0.33636 \times \lambda_{opt}{}^2}{\lambda_{opt}{}^2 - 0.512^2}, \quad (1)$$

and that of DAPC as:

$$n_{opt}{}^2 = 2.459 + \frac{0.17254 \times \lambda_{opt}{}^2}{\lambda_{opt}{}^2 - 0.610^2}, \quad (2)$$

where λ_{opt} is the optical wavelength in μm. The fitted dispersion curves are shown in Fig. 2. Using the formula, at 800 nm, the optical refractive index n_{opt} of both LAPC and DAPC is ~1.70. The optical group index is derived by the following formula:

$$n_g = n_{opt} - \lambda_{opt} \cdot \frac{dn_{opt}}{d\lambda_{opt}}\bigg|\lambda_{opt}. \quad (3)$$

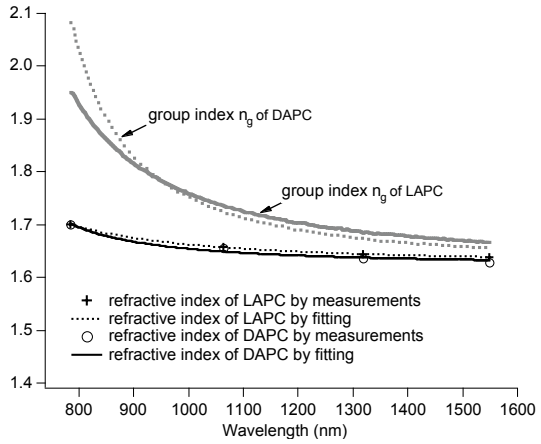

Figure 2: Measured refractive indices of LAPC (pluses) and DAPC (open circles), respectively; fitted refractive indices for LAPC (dotted black line) and DAPC (solid black line), respectively; and calculated group indices for LAPC (dotted gray line) and DAPC (solid gray line), respectively.

For LAPC and DAPC, n_g is approximately 1.93 and 2.03, respectively, at a wavelength of 800 nm. We estimate the THz refractive index n_{THz} of LAPC and DAPC to be ~ 1.68 and ~1.65, respectively, by doing THz-TDS (with a bandwidth of ~8 THz) measurement. Phase-matching for THz generation and detection requires $n_g = n_{THz}$. Obviously, there is no good phase-match for both materials with 800-nm-wavelength light sources. However, the feature of approximately constant n_{THz} for polymers is in contrast to ZnTe (a standard THz emitter/sensor material), where n_{THz} changes dramatically in the range between 0 and 8 THz. This feature is attributed to the lack of phonon resonance in amorphous polymer films and provides us an opportunity to achieve perfect phase-matching for a wide range of THz frequencies, via optical wavelength tuning, which will be presented in Sec. 5.

3. EXPERIMENTS

To study the performance of our THz system in the near-infrared range, we used a regenerative laser amplifier (Spectra Physics Spitfire). The amplifier provides ~30-nm bandwidth, ~50-fs laser pulse duration, and 1-kHz repetition rate. To avoid laser pulse-width broadening from material dispersion, we used only reflective optical elements. The schematic of our experimental set-up is shown in Fig. 3.

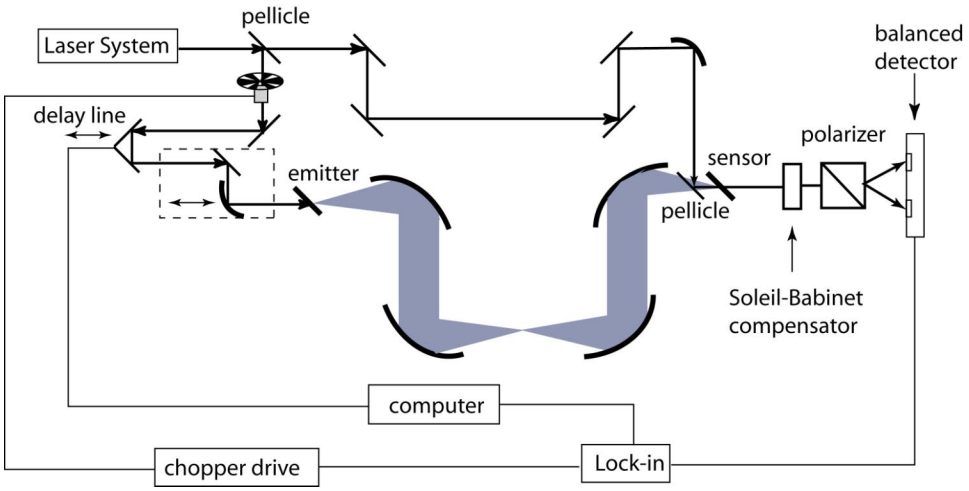

Figure 3: Schematic of the experimental set-up.

Only ~10 mW pump power, measured after the optical chopper was focused by a parabolic mirror (with effective focal length of 50.8 mm) onto a 70-μm LAPC emitter, with an elliptical spot of ~6 mm^2 , to generate THz radiation (via optical rectification). In order to achieve maximum THz emission from the polymer, with a *p*-polarized pump beam, we oriented the polymer film such that the pump beam was incident at Brewster's angle.

We used EO sampling to detect the generated THz radiation. Another LAPC film was used as the EO sensor, where the probe pulses (< 1 mW) traveled collinearly with the THz pulses and the polarization of the probe beam changed due to the transiently changed refractive indices of the EO polymer induced by the existence of the THz field. Because the LAPC films were poled normal to the substrate, and the generated THz field was *p*-polarized, the LAPC film sensor was rotated 45° with respect to the *p*-polarized THz field, providing a projected component of the THz field along the poling direction of the LAPC polymer. This overlap is essential for EO detection. For the best EO detection, the polarization of the probe beam should be kept at 45° with regard to the incidence plane. However, insertion of any half-wave plate to rotate the probe beam polarization would broaden our 50-fs laser pulse-width. Therefore, alternatively, we further rotated the LAPC film until the probe beam polarization was approximately 45° with regard to the incidence plane. With this specific orientation of the LAPC sensor, its effective thickness was >70 μm. A Soleil-Babinet compensator and a Wollaston prism were used to convert the change of probe beam polarization state into the change of beam intensity for differential measurement. We used the conventional balanced detection scheme to achieve a good signal-to-noise ratio.

Figure 4 shows a typical THz amplitude spectrum from the LAPC emitter-sensor pair (solid black line). The result was obtained by averaging 10 time-domain traces and then Fourier transforming the averaged THz wave to the frequency domain. The time constant of the lock-in was set at 100 ms. The observable bandwidth is ~12 THz, free of spectral gaps. For comparison, we replaced the LAPC emitter with an 80-μm ZnCdTe, which has similar properties as ZnTe (a standard EO material for THz generation and detection), and repeated the experiment. The corresponding THz spectrum is shown as the dotted gray line in Fig. 4. There is a strong absorption gap around 5 THz, as is expected due to the phonon resonance of ZnCdTe. The gap-free, broadband THz spectrum from the polymer emitter-sensor pair is especially promising for THz-TDS applications because richer and more complete spectroscopic information can be obtained.

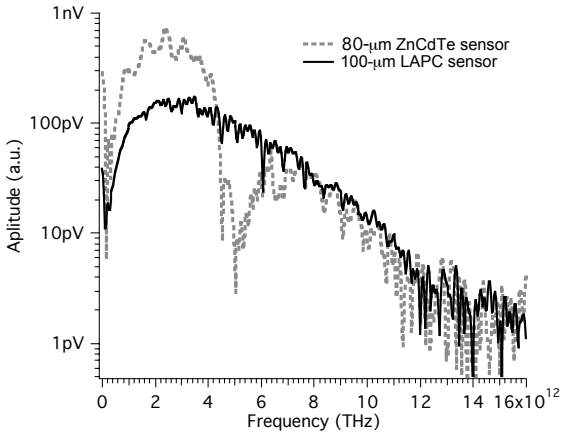

Figure 4: Fourier-transform amplitude spectra of the THz waves generated by a 100-μm thick LAPC emitter and detected by a 180-μm thick LAPC sensor (solid black line) and an 80-μm thick ZnCdTe sensor (dotted gray line), respectively. The spectral gap around ~5 THz is due to the lattice resonance effect in the ZnCdTe crystal.

The water absorption lines above 7 THz are well lined up for both spectra (the air was not completely dry when the experiments were done). Around 2 THz, the ZnCdTe sensor is about 4 times more sensitive than the LAPC sensor, which is due to the fact that a good phase-match exists in this spectral region for ZnCdTe, with the probe beam wavelength at 800 nm. The other reason for the lower sensitivity of LAPC sensor is due to the poling geometry. As explained above, only the projected component, not the full strength of the THz field, is measured. This issue can be solved by turning to in-plane poling geometry in the future. It can also be tackled by using optical wavelengths that lead to smaller phase-mismatch, and above all, by designing and synthesizing polymeric materials with very high EO coefficients and/or smaller phase-mismatch. Multiple internal reflections inside the ~80-μm thick ZnCdTe crystal explain the ~0.7-THz-period spectral modulation. This effect is mostly eliminated in the case of the LAPC sensor due to the oblique incidence of the THz field and the lower refractive index of LAPC.

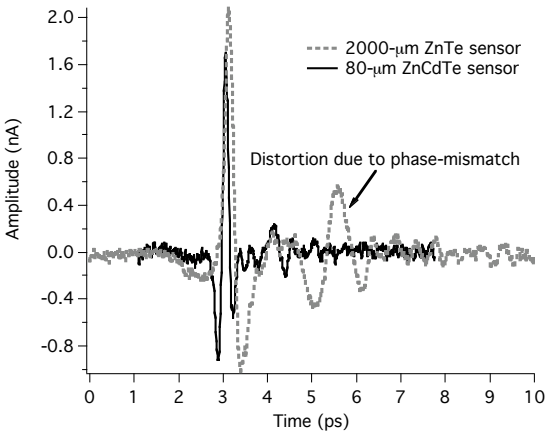

Figure 5: Transient THz radiation generated by a 70-μm DAPC emitter and detected by a 2-mm ZnTe sensor (dotted gray line) and 80-μm ZnCdTe sensor (black line), respectively. The extensive distortion for the 2-mm ZnTe sensor is due to significant phase-mismatch in the sensor.

We then used an OPA, pumped by the regenerative laser amplifier and emitting pulses with wavelengths tunable between 1100 nm and 1600 nm, to investigate the performance of DAPC as the THz emitter. The pump power is ~7 mW (<100 fs, 1 kHz), measured after the chopper. Figure 5 shows the pulsed THz waves generated by the DAPC emitter and

detected by the 80-μm ZnCdTe sensor and 2-mm ZnTe sensor, respectively. The results were obtained when the OPA wavelength was tuned to 1300 nm. Comparing the two traces, we observe an obvious THz wave distortion for the 2-mm ZnTe sensor, resulting from the significant phase-mismatch between the transient THz wave and the 1300-nm-wavelength probe pulse. The use of the 80-μm ZnCdTe sensor reduced the detection distortion. The corresponding THz spectra are shown in Fig. 6. In the case of the 80-μm ZnCdTe sensor, we observe an overall bandwidth of ~ 5 THz with a flat part between ~1 THz and ~3.5 THz. The bandwidth cut-off at ~5 THz can be explained by the phonon absorption of ZnCdTe. The periodic modulation of the spectrum is attributed to the internal refection of the THz wave inside the ZnCdTe crystal. On the other hand, for the 2-mm ZnTe sensor, although the observable bandwidth is still ~5 THz, limited by the lattice resonance of ZnTe, there are some obvious spectral dips. Since both experiments were carried out in the purged dry air, these dips cannot be explained by the water absorption. In addition, we did not scan our optical delay line far enough to see the THz reflection from the exit surface of the 2-mm ZnTe crystal. We believe the spectral dip are associated with the phase mismatch effect.

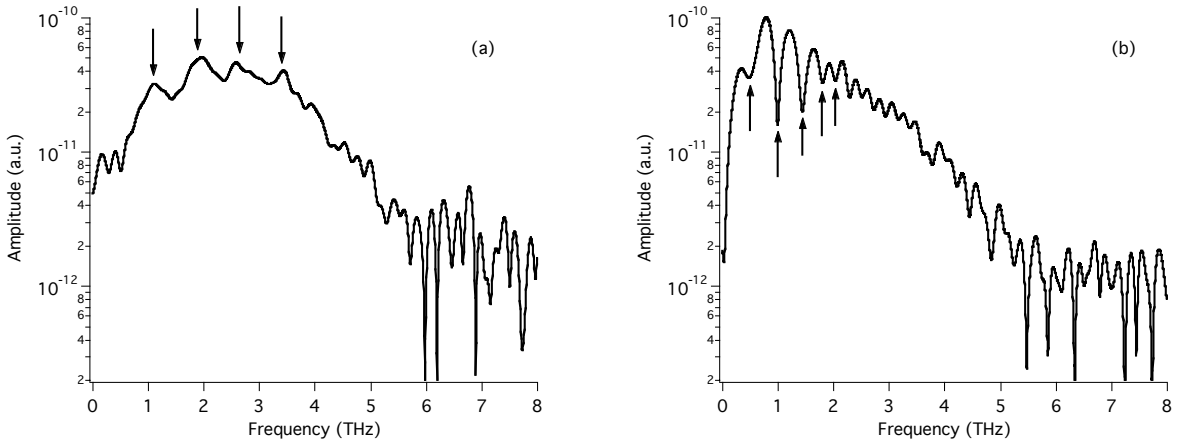

Figure 6: Amplitude spectra of the THz radiation generated by a 70-μm DAPC emitter and detected by a 80-μm ZnCdTe sensor (a) and 2-mm ZnTe sensor (b), respectively. The periodic modulation on the spectrum for the 80-μm ZnCdTe is due to the internal reflection of THz wave in the crystal, while the spectral dips on the spectrum for the 2-mm ZnTe results from the phase-mismatch.

4. MODELING

THz emission in an EO medium is driven by the nonlinear polarization induced by the difference frequency mixing process between the spectral components of an ultrashort laser pulse $E_{pump}(\omega,z)$. Mathematically, this propagating nonlinear polarization along the z-axis is described by:

$$\begin{aligned} P_{OR}(\Omega,z) &= \int_{-\infty}^{\infty} \chi_{eff}(\Omega;\omega,-\omega+\Omega) E_{pump}(\omega,z) E_{pump}^{*}(\omega-\Omega,z)\, d\omega \\ &= \chi_{eff}(\Omega) \int_{-\infty}^{\infty} E_{pump}(\omega,z) E_{pump}^{*}(\omega-\Omega,z)\, d\omega, \end{aligned} \tag{4}$$

where Ω and ω are the THz and optical frequency, respectively and it is assumed that the effective nonlinear susceptibility χ_{eff} is independent of optical wavelength for our polymer films over the bandwidth of the pump and probe pulses. The assumption is justified since the pump wavelength of 800 nm is away from the electronic resonance region of LAPC and DAPC. Furthermore, for amorphous polymer films, χ_{eff} is approximately constant in the THz regime, due to the lack of lattice resonance. We now have a full description for the OR effect in an EO medium:

$$\frac{\partial^2 E_{THz}(\Omega,z)}{\partial z^2}+\frac{n_{THz}^2\cdot\Omega^2}{c^2}E_{THz}(\Omega,z)=-\frac{4\pi}{c^2}\cdot\chi_{eff}\cdot\Omega^2\cdot P_{OR}(\Omega,z), \tag{5}$$

where E_{THz} is the THz wave and c is the speed of the light. We have reduced the conventional three-dimension nonlinear equation to an one-dimension one, based on the fact that the thickness of LAPC polymers is much smaller than the Rayleigh length of both THz and laser fields. We have also taken the assumption that laser field depletion and absorption by the EO medium can be neglected. The former assumption eliminates the need to solve the coupled nonlinear equations involving the evolution of both pump and newly generated waves, usually encountered in multi-wave mixing processes, such that we can solve only Eqn. (5) to obtain THz field. The latter assumption is just for the simplification of the problem for the time being and can be included into the model if needed.

Only the expression of the laser field is needed in order to solve this equation. In the modeling work by Faure *et al.*,[13] it is assumed that the laser pulse width does not change when it propagates along an EO medium. We think it doesn't hold true for LAPC since 800 nm is located on the absorption falling edge of our polymers, leading to quite some group index dispersion (Fig.2) that broadens the laser pulse width. With the group index dispersion taken into consideration and transfer-limited incident pulses assumed, the propagating laser field in an EO medium is:

$$E_{pump}(z,t)=\frac{1}{2}E_o\cdot\frac{T_o^2}{T_o^2-i\beta_2 z}\cdot\exp[-\frac{(t-z/v_g)^2}{2(T_o^2-i\beta_2 z)}]\cdot\exp(-i\omega_o t+ik_o z)+c.c., \tag{6}$$

where E_o is the amplitude of the laser field, T_o is the half-width of the pulse at 1/e of its intensity ($\propto E^2$), v_g is the group velocity of laser pulse at center wavelength in the medium, ω_o and k_o are the center frequency and the corresponding wave vector, respectively, and $\beta_2=\frac{d^2k}{d\omega^2}=\frac{\lambda^3}{2\pi\cdot c^2}\cdot\frac{d^2n}{d\lambda^2}$ is the group index dispersion coefficient of the medium (determines how fast a laser pulse broadens when propagating in a medium). Using Eqn. (1) and (2), β_2 can be calculated to be 1.859 $fs^2/\mu m$ and 3.994 $fs^2/\mu m$ for LAPC and DAPC, respectively, at wavelength of 800 nm. Obviously, laser pulse width broadens faster in DAPC than in LAPC. It is straightforward to Fourier-transform the expression in Eqn. (6) to the frequency domain in order to solve the nonlinear Eqn. (5). However, because of the complexity of the expression of the laser field, there is no analytical solution for Eqn. (5). For this reason, we numerically solve it to obtain $E_{THz}(\Omega,z)$.

As for the THz detection by an EO sensor, we employed the existing model developed by Gallot *et al.*[14] and included the pulse width broadening into the model to calculate the response function of an EO sensor $f(\Omega,d_{sensor})$. Therefore, in this modified model, all the effects such as broadening of the laser pulse, material absorption and dispersion, sensor thickness d_{sensor} and phase-mismatch are considered. $S_{THz}(\Omega,d_{emitter},d_{sensor})=E_{THz}(\Omega,d_{emitter})\cdot f(\Omega,d_{sensor})$ is the simulated electric field from a THz system based on optical rectification and EO sampling , with THz propagation effects neglected at this point.

Using this model, we simulated the THz spectrum obtained from our LAPC emitter-sensor pair. All the parameters used in the simulation were consistent with the real experimental conditions. Figure 7 shows the simulation result and the comparison with the experimental result. Both the simulation and the experiment exhibit bandwidth of ~12 THz. However, the peak frequency obtained from the experiment is lower than that from the simulation. We believe that water vapor absorption lowers the amplitude for the higher frequency components and causes the peak frequency to be shifted towards the lower end. It is well know that there exists strong water absorption in the THz range. The air in our experiment was not completely dry, which is evident in the experimentally obtained spectrum in Fig. 7.

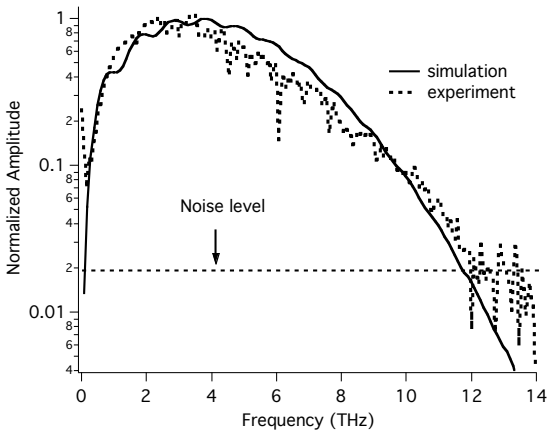

Figure 7: Comparison for the simulated and experimentally obtained THz spectra of the THz system based on a LAPC emitter and sensor pair. For simulation, the emitter thickness was assumed to be 80 μm, the sensor thickness to be 100 μm, the central wavelength of the laser pulse to be 800 nm, and the pulse width to be 53 fs (FWHM). Both spectra exhibit bandwidth up to ~12 THz. The slight difference of peak frequency might be due to water absorption in the experiment.

We also did simulation for DAPC emitter and ZnCdTe/ZnTe sensor with 1300-nm-wavelength pulses. In the case of the 80-μm ZnCdTe sensor, the THz spectrum from the simulation (solid black line of Fig. 8) is flat up to 3.5 THz, which is consistent with the experiment (gray dotted line of Fig. 8). Since we did not include the effect of reflection in our model, it is not surprising that our simulation result does not show the spectral modulation that exhibits in the experimental result. For the discrepancy that occurs above 4 THz, we blame the lack of an model that can accurately predict the THz refractive indices around the lattice resonance (~ 5.3 THz for ZnTe). In our modeling, we used the refractive index model presented by Gallot *et al.*[15] As for the 2-mm ZnTe sensor (Fig. 9), the simulation shows phase-mismatch induced spectral dips, the first a few dips line up well with the experimental result. Like the 80-μm ZnCdTe sensor, most of the discrepancy between the experiment and simulation occurs around the lattice resonance range.

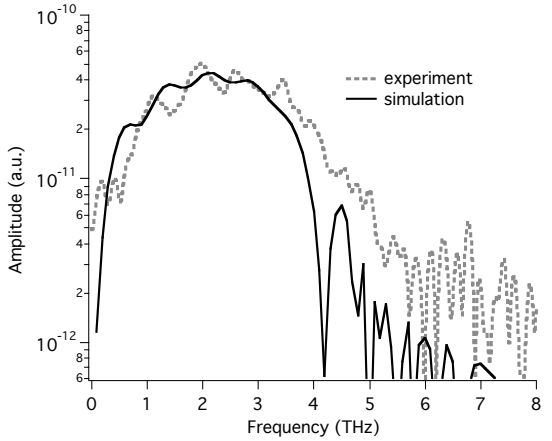

Figure 8: THz amplitude spectra predicted by modeling (solid black line) and measured by the experiment (dotted gray line), respectively, with a 70-μm DAPC emitter and 80-μm ZnCdTe sensor pair used.

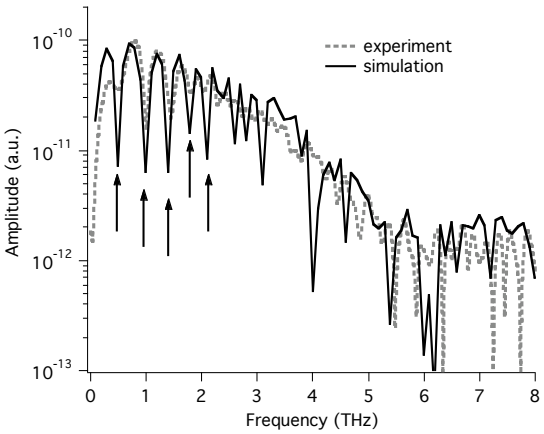

Figure 9: THz amplitude spectra predicted by modeling (solid black line) and measured by the experiment (dotted gray line), respectively, with a 70-μm DAPC emitter and 2-mm ZnTe sensor pair used.

5. DISCUSSION

Both the experiments and simulations have shown that ZnTe and ZnCdTe are not suitable materials for THz systems when one tries to get broad bandwidth using infrared pulses that can be easily obtained from compact and maintenance-free fiber lasers. The reason for this is that there is no good phase-matching existing for these materials in the infrared range, not to mention the issue of the phonon absorption gap. It has been shown that a good phase-matching for ZnTe can only be achieved in the near infrared range around 800 nm. On the other hand, polymer engineering provides us a wide variety of material possibilities, some of which exhibit very high EO coefficients and good phase-match for THz emission and detection at certain optical wavelengths.

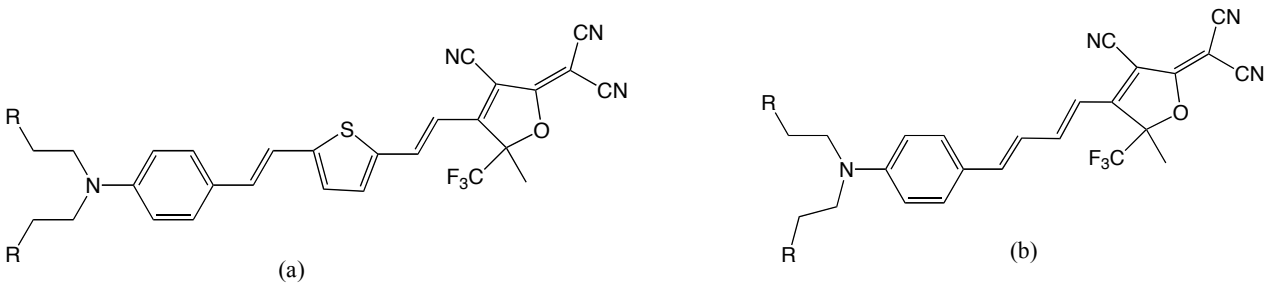

Figure 10: Chemical structure of (a) AJL8 and (b) AJN110.

Recently, we have identified EO polymers with chromophore dopants of AJL8 and AJN110, respectively, promising for THz applications using infrared light sources. They are the recent achievement of advanced chromophore design towards extremely high nonlinearity for such applications as optical modulators and switches.[16] The chemical structures of the chromophore AJL8 and AJN110 are shown in Fig. 10(a) and Fig. 10(b), respectively. AJL8 and AJN110 mixed with APC exhibit EO coefficients of 65 pm/V and 61 pm/V, respectively, in contrast to 18 pm/V for DAPC used in our experiments at 1300 nm. The wavelength tunability of OPA provides an opportunity to achieve good phase-matching for the two new polymer composites. Figure 11 shows the dispersion curves of the optical group indices for DAPC, AJL8/APC and AJN110/APC, respectively. The latter two polymers show very similar optical properties, with group index changing from 1.78 at 1100 nm to 1.63 at 1600 nm. Our previous THz-TDS study has shown that the THz index of DAPC is in between these two values. Since the THz index of AJL8/APC and AJN110/APC should not be very different from APC, we can reach a point, by tuning the OPA wavelength, where the THz index and the optical group index equal to each other. In other words, by wavelength tuning, we can achieve perfect phase-match. This picture can

be best seen by our simulation results shown in Fig. 12, based on the model presented above. The best phase-match for AJL8 occurs around 1500-nm wavelength if the THz index of 1.65 is assumed (the measurement to evaluate the exact value will be done in the near future). Also shown in Fig. 12 are the simulated THz spectra for DAPC emitter-sensor pair with different optical wavelengths. It is obvious that a broader observable bandwidth can be achieved for AJL8/APC when the same minimum detection level (determined by the whole system noise level) is assumed, since AJL8/APC with the higher EO coefficient makes a more efficient emitter and more sensitive sensor. Therefore, the ever increasing EO coefficient from novel polymeric materials opens the door to bright and broadband THz sources and detectors that can not be achieved from any crystalline EO material.

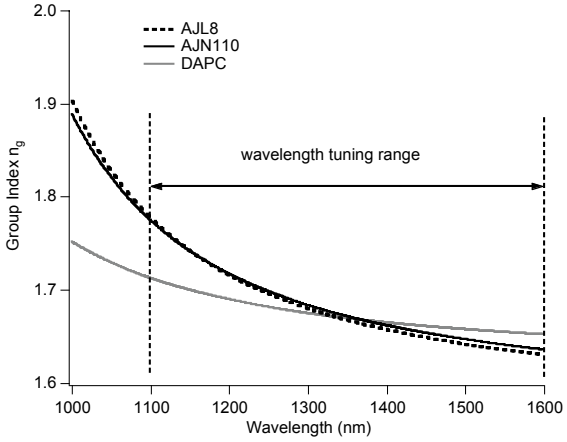

Figure 11: Group indices n_g of AJL8, AJN110, and DAPC, respectively, in infrared range. The output wavelength from our OPA is tunable from 1100 nm to 1600 nm.

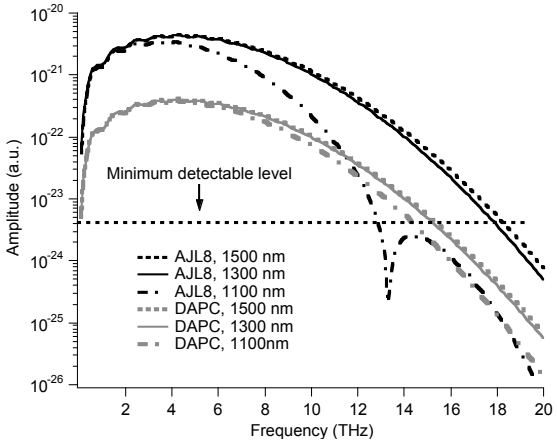

Figure12: Simulation for the achievable bandwidths of AJL8/APC and DAPC with different optical wavelengths. A hypothetical line for minimum detectable level is used to show that the achievable bandwidth depends on both EO coefficient and phase-match condition of polymers. AJL8, with much higher EO coefficient than DAPC, is capable of providing broader bandwidth if the wavelength is tuned at the point where it is well phase-matched.

ACKNOWLEDGEMENTS

This work is supported by the National Science Foundation (ECS-0139457) and partially by the STC-MDITR program of the National Science Foundation (DMR 0120967).

REFERENCES

1. K. P. Cheung D. H. Auston, and P. R. Smith, Appl. Phys. Lett. **45**, 284 (1984).
2. Ch Fattinger and D. Grischkowsky, Appl. Phys. Lett. **54**, 490 (1989).
3. D. H. Auston and M. C. Nuss, IEEE J. QE **24**, 184 (1988).
4. Q. Wu and X.-C. Zhang, Appl. Phys. Lett. **67**, 3523 (1995).
5. Q Wu and X.-C Zhang, Appl. Phys. Lett. **71**, 1285 (1997).
6. K Liu, J. Xu, and X.-C. Zhang, Appl. Phys. Lett. **85**, 863 (2004).
7. C. Kubler, R. Huber, S. Tubel, A. Leitenstofer, Appl. Phys. Lett. **85**, 3360 (2004).
8. Y. C. Shen, P. C. Upadhya, H. E. Beere, E. H. Linfield, A. D. Davies, I. S. Gregory, C. Baker, W. R. Tribe, and M. J. Evans, Appl. Phys. Lett. **85**, 164 (2004).
9. Y. Shi, C. Zhang, H. Zhang, J. H. Bechtel, L. R. Dalton, B. H. Robinson, and W. H. Steier, Science **288**, 119 (2000).
10. A. M. Sinyukov and L. M. Hayden, Opt. Lett. **27**, 55 (2002).
11. A. M. Sinyukov, M. R. Leahy, L. M. Hayden, M. Haller, J. Luo, A. K. -Y. Jen, and L. R. Dalton, Appl. Phys. Lett. **85**, 5827 (2004).
12. H. Cao, T. F. Heinz, and A. Nahata, Opt. Lett. **27**, 775 (2002).
13. J. Faure, J. van Tilborg, R. A. Kaindl et al., Optcial and Quantum Electronics **36**, 681 (2004).
14. G. Gallot and D. Grischkowsky, J. Opt. Soc. Am. B **16**, 1204 (1999).
15. G. Gallot, J. Zhang, R.W McGowan, T. -I. Jeon, and D. Grischkowsky, Appl. Phys. Lett. **74**, 3450 (1999).
16. G. T. Paloczi, Y. Huang, A. Yariv, J. Luo, and A. K. -Y. Jen, Appl. Phys. Lett. **85**, 1662 (2004).